I&EC research
Industrial & Engineering Chemistry Research

Article

pubs.acs.org/IECR

Hydrogenation of Tetralin over Ir-Containing Mesoporous Catalysts

Verónica A. Vallés, Gerardo S. Balangero Bottazzi, María L. Martínez, Marcos B. Gómez Costa, Oscar A. Anunziata, and Andrea R. Beltramone*

Centro de Investigación en Nanociencia y Nanotecnologia (NANOTEC), Facultad Regional Córdoba, Universidad Tecnológica Nacional, Maestro López y Cruz Roja Argentina, 5016, Córdoba, Argentina

ABSTRACT: A new series of catalysts based on noble metals have been prepared with the main aim of obtaining thiotolerant catalysts to be used in second-stage processes of mild hydrotreating. We studied the catalytic properties of 1 wt % Ir-containing mesoporous materials in the hydrogenation of tetralin to decalin, in the presence of 100 ppm of dibenzotiophene at 250 °C and 15 atm pressure of hydrogen, using a Parr reactor. Ir/mesoporous materials were prepared by wetness impregnation, using iridium acetylacetonate as the source of Ir. The Ir/SBA-3 catalyst synthesized by us had a high activity in tetralin hydrogenation under mild conditions. The experimental data were quantitatively represented by a modified Langmuir−Hinshelwood-type rate equation. The preliminary results reveal that these materials are promising catalyts for HDS/HDN reactions.

INTRODUCTION

The yield in fluid catalytic cracking (FCC) depends on the extent of aromatic hydrogenation in the gas oil hydrotreater. To optimize the gas oil hydrotreater, it is crucial to understand the aromatic hydrogenation reaction chemistry occurring in the gas oil hydrotreater. Gas oils, which consist of hydrocarbons in the boiling point range of 290−570 °C, contain several aromatic compounds (including three rings, two rings, and one ring). Light cycle oil (LCO), which contains large concentrations of aromatics, has a poor cetane value and, hence, by itself, is a very poor-quality diesel. Because the current regulations [on cetane and polynuclear aromatic (PNA) hydrocarbons] are not stringent, LCO is currently blended with diesel. However, it is anticipated (based on existing regulations in Europe and California) that diesel quality in the near future will be more stringently regulated in terms of cetane and aromatics. To find alternative processes, it is necessary to develop new and more active catalysts to replace the current ones. Optimal design and operation of such hydrogenation processes can be achieved through the use of reliable simulation tools; however, such tools require detailed knowledge of kinetic pathways and rates.[1−3] Kinetic experiments on hydrogenation are typically performed in the gas phase under atmospheric pressure on group VIII metal catalysts. Previously, Beltramone et al.[4,5] reported a detailed study and a quantitative network analysis of polynuclear aromatics aromatization at industrial conditions, and Korre and Klein[6] reported an exhaustive study in a batch reactor at high pressure.

Otherwise, the sulfur and nitrogen compounds found in synthetic feedstocks and heavy petroleum fractions can strongly inhibit hydroprocessing reactions through competitive adsorption. The presence of these species even at low concentrations can limit the observed catalytic activity and necessitate the use of higher pressures and temperatures to obtain desired conversions. Therefore, the need for more active catalysts is crucial in this process. The development of highly active and selective hydrotreating catalysts is one of the most pressing problems facing the petroleum industry.

Current processes for dearomatization use catalysts combining the acidity of a support and the hydrogenation and hydrogenolysis/ring-opening activity of an incorporated metal. Hydrogenation/hydrocracking is most often practiced on cyclic molecules over primarily acidic zeolite, alumina, or silica-alumina-supported noble and other group VIII metal catalysts. Different processes have used catalysts such as NiMo, CoMo, NiW, Pt, and Pd on various supports.[7−17] The dominance of the acid function can lead to cracking, and thus, a primary focus is the optimization of the acid function. In fact, it was shown recently that significant enhancements in hydrogenation can be made by focusing on the metal function. The metal function is usually provided by Pt and/or Pd, but it has been shown that Ir, Ru, and Rh also have exceptional activities and selectivities for the target reaction of hydrogenation and, depending on the reaction conditions, selective ring-opening.[18−20] Some alumina-supported transition-metal catalysts have much higher hydrodenitrogenation (HDN) and hydrodesulfurization (HDS) activities than the conventional NiMo system.[21−25] For example, Rh, Ir, Ru, and Pt supported on silica or alumina are known to effectively catalyze nitrogen removal from methylamine, quinoline, or pyridine also in the reduced state.[26] Noble-metal sulfides, either unsupported as bulk compounds[27] or supported on active carbon,[28] have been studied extensively in hydrorefining. It has been shown that transition-metal sulfides of the second and third rows such as those containing Ru, Rh, Os, and Ir are especially active during HDS reactions.[27] Similarly, sulfides of Ir, Os, and Re were found to be most active in the HDN of quinoline,[28] and sulfides of Ir and Pt were found to be most active in the HDN of pyridine.[29] However, catalytic properties of metal deposited on alumina or other supports have been studied less frequently, and moreover, the primary attention to date has been devoted only to Ru.[30] It was shown by Cinibulk and Vít[31] that the HDN

Received: November 23, 2011
Revised: March 21, 2012
Accepted: April 21, 2012
Published: April 21, 2012

dx.doi.org/10.1021/ie202727r | *Ind. Eng. Chem. Res.* 2012, 51, 7185−7195

activity of an alumina-supported Ir catalyst during the parallel HDN/HDS reaction of pyridine and thiophene was markedly higher than the activity of a Pt catalyst and that modifcation of a NiMoP/alumina catalyst by 0.5% Ir increased the C−N bond hydrogenolytic activity by a factor of 2.[32] In addition to HDN, a high hydrogenolytic activity of Ir has also been well-established during studies of hydrocarbon reactions in connection with naphtha reforming.[33,34]

Regarding new support materials, mesoporous molecular sieves such as MCM-41, HMS, and SBA-15[35−38] are promising candidates because of their uniform mesoporous structure, which facilitates the diffusion of the large molecules involved in hydrotreating reactions. Nava et al.[39] successfully used CoMo/Ti-SBA-15 catalysts for dibenzothiophene desulfurization, but information about SBA-16 and SBA-3 supports is scanty or nonexistent. In 1998, Zhao et al.[40] synthesized a new type of mesoporous material called SBA, with a uniform two-dimensional hexagonal structure; this material is characterized by larger pores up to approximately 25 nm that allow bulky molecules to enter into the pores, among different supports with ordered pore structure.[41] Many investigations have indicated that Al-SBA-15 materials show much higher catalytic activity than Al-MCM-41 material.[42] Two methods including direct synthesis and postsynthesis have been developed to incorporate Al into the frameworks of mesoporous materials. However, direct synthesis seems infeasible for some materials such as SBA-15,[43] because the majority of aluminum precursors will dissolve in the strong acidic media used during the synthesis procedure. Previous works on postsynthesis for alumination of the SBA family[43−45] showed that this process is well-adapted to some mesoporous materials. The synthesis of SBA-3 mesostructured silica containing framework aluminum was previously reported by us.[46] This material was successfully synthesized using sodium aluminate through a postsynthesis method. It can be expected that this structure offers more interesting opportunities for catalytic applications involving well-dispersed metal-supported catalysts and allowing the diffusion of large molecules. The SBA-16 silica mesophase with a cubic *Im*3*m* structure was prepared first by Zhao et al.[40,47] from the triblock copolymer surfactant Pluronic F127 ($EO_{106}PO_{70}EO_{106}$, where EO = ethylene oxide and PO = propylene oxide) and tetraethylorthosilicate (TEOS). The synthesis parameters were systematically investigated by Mesa et al.[48] The mesoporosity of this phase consists of two noninterpenetrating three-dimensional channel systems with spherical cavities at the dividing of the channels.

To saturate aromatic hydrocarbons, conventional hydrotreating catalysts based on Co−Mo, Ni−Mo, or Ni−W sulfides supported on alumina must work under severe operating conditions, which increases the process costs.[49] In this case, noble-metal-based catalysts are an interesting alternative, because they have high activity for hydrogenation of aromatic hydrocarbons and the process could then be performed at low temperatures and pressures.

It should be noted that studies devoted exclusively to monometallic Ir catalysts in relation to hydrotreating are very rare.[31,50,51] More often, studies have involved comparisons of monometallic Ir and Pt catalysts.[52−56] However, the bulk of such articles have studied iridium sulfide together with a series of other noble-metal sulfides. The Ir catalysts have often been used in the form of sulfides, whereas in about 20% of the studies, they were reduced to the metal.

Factors such as the effects of catalyst preparation and metal dispersion have often been studied in connection with this process.[57−60] The results obtained in all of these studies suggest that Ir could be an efficient active phase for the transformation of aromatics to saturated compounds and for sulfur and nitrogen removal, either by itself or as a promoter of conventional catalysts. However, data about the effects of Ir dispersion in different supports in hydrogenation reactions are not available in the literature at present. The metal particle size of supported metal catalysts is an important factor affecting catalytic behavior, and the support, particularly the pore structure, can affect the metal dispersion. A preparation method leading to a mesoporous matrix with controlled low acidity was previously reported.[46] In a previous work,[61] we demonstrated the good performance of Ir/SBA-16, studying the catalytic properties of 5 wt % Ir-containing SBA-16 catalysts (with and without aluminum as a heteroatom), in the hydrogenation of tetralin to decalin, in the presence of nitrogen and sulfur compounds. The 5 wt % Ir/SBA-16 catalyst synthesized by us had high activity in tetralin hydrogenation under mild conditions.

In this article, we describe the preparation of new mesoporous catalytic materials containing highly and homogeneously dispersed reduced particles of Ir^0 and investigate their activity for hydrogenation of aromatic compounds, using tetralin as a model substrate under mild conditions in a batch reactor.

Langmuir−Hinshelwood-type rate equations were used to describe the reaction kinetics with physically meaningful and well-identified parameter values.

EXPERIMENTAL SECTION

Synthesis of Si-SBA-16. Mesoporous silica materials with the cubic *Im*3*m* structure were synthesized according to the procedure described in ref 62. Briefly, poly(alkylene oxide)-type triblock copolymer, Pluronic F127 ($EO_{106}PO_{70}EO_{106}$, MW 12600), was dissolved in aqueous HCl solution. Tetraethyl orthosilicate was added to the solution at 35 °C under continuous stirring during 15 min at that temperature. The molar composition of the mixture was F127/TEOS/HCl/H_2O = 0.004:1:4:130. This mixture was kept under static conditions in an oven for 6 h at the same temperature. Subsequently, the mixture was placed in an oven at 50 °C over a period of 20 h; afterward, the temperature of furnace was increased to 80 °C for aging for 20 h, and then, the solid product was recovered by filtration and dried at 100 °C. The Si-SBA-16 sample was immersed in refluxing ethanol for 6 h to extract the surfactant, which was then calcined at 550 °C in air for 6 h. The material obtained was identified as SBA-16.

Synthesis of Si-SBA-3 and Na−Al-SBA-3. Mesoporous aluminosilicate was synthesized by hydrolysis of tetraethylorthosilicate (TEOS) and sodium aluminate at room temperature, in aqueous acidic solution, using cetyltrimethylammonium bromide (CTAB) as the surfactant. The designed procedure was as follows: The surfactant was mixed with water and HCl; then, 3 g of TEOS was added under stirring to form a mixture with a molar composition of TEOS/H_2O/HCl/CTAB = 1:130:9.2:0.12.[46] After 45 min, a white precipitate was obtained, which was then filtered, washed, and dried at room temperature. The material was immersed in refluxing ethanol for 6 h to extract the surfactant. The sample was then calcined at 450 °C in air for 6 h. The material obtained was denoted as SBA-3. The alumination procedure of SBA-3[43,63] was carried

dx.doi.org/10.1021/ie202727r | Ind. Eng. Chem. Res. 2012, 51, 7185−7195

out as follows: Silica-SBA-3 (1 g) was stirred in 50 mL of water containing dissolved sodium aluminate in different proportions at room temperature for 20 h. The mixture was filtered, washed, dried at room temperature overnight, and then calcined in air at 450 °C for 5 h. Finally, an Al-SBA-3 sample with Si/Al = 20 was obtained.

Synthesis of MCM-41. Typical MCM-41 mesoporous material[64] was synthesized by dissolving 2.4 g of *n*-cetyltrimethylammonium bromide (CTAB, Aldrich) in 120 g of deionized water and stirring until the solution was homogeneous and clear. After 8 mL of ammonium hydroxide (Merck) had been added, the mixture was stirred for 5 min, and then 10 mL of TEOS (Merck) was added. The molar composition of the gel was 1 M TEOS/1.64 M NH_4OH/0.15 M CTAB/126 M H_2O. The reaction mixture was stirred overnight, and then the solution was filtered and washed consecutively with deionized water and ethanol. Calcination was performed at 550 °C for 5 h, yielding fine particles of MCM-41.

Synthesis of Ir/Mesoporous Materials. We concentrate here on the direct incorporation of iridium by wetness impregnation of the calcined form followed by thermal treatment and reduction under hydrogen. We used iridium acetylacetonate [$Ir(acac)_3$, Aldrich, 99.9%) as the source of Ir, with ethanol as the solvent, because of the very low solubility of $Ir(acac)_3$ in water. The obtained powder was then dried at 80 °C overnight and calcined at 500 °C for 5 h. After that, the samples were desorbed in an inert atmosphere from 25 to 200 °C at a rate of 10 °C/min and kept at 200 °C for 5 h, after which the temperature was increased to 470 °C at a rate of 10 °C/min and kept for 5 h at that temperature. The nitrogen flow was always 20 mL/min. Because iridium is active for the reaction in its metallic state, it was reduced in a H_2 flow of 20 mL/min at 470 °C using the same procedure as described above. The iridium loading was 1 wt %, and the catalytic materials obtained were identified as Ir/SBA-16, Ir/SBA-3, Ir/Al-SBA-3, and Ir/MCM-41.

Characterization of the Catalysts. The X-ray diffraction (XRD) patterns were collected using a continuous scan mode with a scan speed of 0.02° (2θ)/min. XRD patterns were recorded in a Philips X'Pert PRO PANalytical diffractometer, operating with Cu Kα X-ray radiation (X-ray generator current and voltage set to 40 mA and 45 kV, respectively), using small divergence and scattering slits of $^1/_{32}$ mm and a goniometer speed of 1.2° (2θ) min^{-1}. The scanning range was set between 0.5° and 5°. The sample was crushed before analysis and placed in an aluminum sample holder. XRD data were recorded in the range of 40−50° 2θ, which corresponds to the region of the metal (111) reflection. The breadth of this line (full width at half-height) allowed a first estimation of the average metal particle size using the Scherrer relation, eq 1,[65] considering contributions from particle stress and instrumental broadening to be negligible

$$d = \frac{K\lambda}{\beta\cos(\theta)} \quad (1)$$

Here, d is the mean size of the ordered (crystalline) domains (the crystal average size defined as the cube root of the material volume). Furthermore, λ is the X-ray wavelength (1.54 Å), β is the full width at half-maximum (fwhm, in radians) of the same diffraction peak, and θ is the Bragg angle. The Scherrer constant, K, is a dimensionless shape factor that depends on the shape of the nanocluster (and has a typical value of about 0.89), and if the clusters are not spherically shaped, it depends on the (hkl) index of the diffraction peak and has a value of 0.83,[66] although this was not the case in this work.

Transmission electron microscopy (TEM) observations were performed with a Philips CM 200 UT transmission electron microscope at Centro Atómico Bariloche, San Carlos de Bariloche, Argentina. Samples for TEM were prepared by dispersing a small amount of powder in ethanol and depositing a drop of the resulting suspension on a commercial carbon-coated copper grid.

Elemental analysis was performed by inductively coupled plasma-atomic emission spectroscopy (ICP-AES; VISTA-MPX) operated with high-frequency emission power of 1.5 kW and plasma air flow of 12.0 L/min. The surface area was determined by the Brunauer−Emmett−Teller (BET) method using a Micromeritics Chemisorb 2720 apparatus equipped with a thermal conductivity detector (TCD).

Hydrogen chemisorption characterization was performed in a Micromeritics ChemiSorb 2720 instrument, measured at temperature pulses and at atmospheric pressure. The samples were previously treated and reduced. For hydrogen chemisorption, we assumed a stoichiometric value of 2H per Ir. The catalyst (0.5 g) was reduced in situ with H_2 (30 mL/min) at 400 °C for 2 h and purged with N_2 (25 mL/min) at 400 °C for an additional 0.5 h. The samples were cooled to 22 °C and titrated with H_2 pulses in a stream of N_2 until a constant output TCD signal indicated saturation. The mean diameter of the Ir particles was estimated under the simplied assumption of 2H/Ir stoichiometry and a spherical shape of the metal particles.

The nature (Brønsted and Lewis sites) and acid strength of the samples were determined by pyridine (Py) adsorption/desorption. The samples were desorbed at 400 °C for 2 h (4.2×10^{-2} mbar). Pyridine (5 Torr) was adsorbed at room temperature overnight. Then, it was desorbed for 1 h in a vacuum (2.6×10^{-2} mbar) at room temperature and at 100, 200, 300, and 400 °C. Fourier transform infrared (FTIR) spectra of the samples were obtained from self-supported wafers in a vacuum cell with CaF_2 windows.

Catalytic Activity. The catalytic activity was measured in a Parr 4563 reactor system at 250 °C, 15 atm of pressure of hydrogen, and 360 rpm. The feed consisted of 50 mL of 5% v/v of tetralin (98.5%, Fluka) in dodecane in the presence of 100 ppm of S as dibenzothiophene (DBT). The products were analyzed with a HP 5890 Series II gas chromatograph and an HP-5 column. The results were compared with a typical hydrotreatment catalyst ($NiMo/Al_2O_3$, Criterion DN-200). This catalyst was first pretreated in a continuous-flow reactor at atmospheric pressure, in a flow of 10% H_2S in H_2 at 200 °C for 1 h and at 370 °C for 4 h, with a heating ramp of 10 °C/min. For each step, a flow of at least 5 times the stoichiometric number of moles of H_2S required to sulfide the metal components of the catalyst was used. Then, the catalyst was cooled in a flow of nitrogen to room temperature. After the pretreatment, the catalyst was transferred to the batch reactor under a nitrogen atmosphere to avoid contact with air.

RESULTS AND DISCUSSION

Characterization of the Catalysts. *XRD.* For determination of the structure and symmetry of the materials, XRD patterns were analyzed. SBA-16 with a cubic *Im*3*m* structure is a body-centered-cubic arrangement of cages with eight apertures to the nearest neighbors. The unit-cell parameter, a_0, of the crystallographic structure was obtained by solving the

dx.doi.org/10.1021/ie202727r | Ind. Eng. Chem. Res. 2012, 51, 7185−7195

following equation depending on the type of space group: $a_0 = d_{hkl}Q_{hkl}^{1/2}$, where $Q_{hkl} = h^2 + k^2 + l^2$ for a cubic space group such as that of the body-centered-cubic ($Im3m$) SBA-16. A typical X-ray diffractogram of SBA-16 is expected to present peaks at $2\theta < 3°$, corresponding to an $Im3m$ cubic structure;[40,67] however, often, just the first two peaks have been clearly detected.[68,69] The X-ray diffractograms of SBA-16 and Ir-SBA-16 are shown in Figure 1. The XRD pattern of calcined SBA-16 sample shows

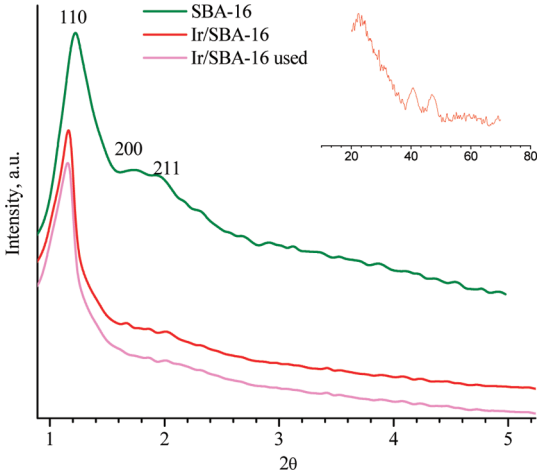

Figure 1. XRD patterns of synthesized SBA-16 and Ir/SBA-16 samples. Inset: High-angle XRD of Ir/SBA-16.

a very strong (110) reflection (1.2° 2θ) of the cubic $Im3m$ structure and two small shoulders of the (200) and (211) reflections (1.7° and 1.92° 2θ, respectively). All of these reflections yield an a_0 value of 12.16 nm (Table 1), confirming that the measured structure is indeed the $Im3m$ structure.[70,71]

Table 1. Physicochemical and Structural Properties of the Supports and Catalysts

	Si/Al[a]	a_0 (nm)	area (m^2/g)	Ir[a] (wt %)	D^b (%)	average size of the metallic clusters (nm)
SBA-16	–	12.16	870	–	–	–
Ir/SBA-16	–	12.4	560	0.92	48	2.4,[b] 2.6[d]
SBA-3	–	3.69	1024	–	–	–
Ir/SBA-3	–	3.74	758	1.02	77	1.5,[b] 1.6,[c] 1.7[d]
Al-SBA-3	19.8	4.2	770	–	–	–
Ir/Al-SBA-3	19.8	4.19	598	0.95	64	1.8,[b] 2.1,[c] 2.2[d]
MCM-41	–	4.09	1235	–	–	–
Ir/MCM-41	–	4.55	915	1.12	55	2.1,[b] 1.9,[c] 2.3[d]
Ir/Al_2O_3	–	–	162	0.99	33	3.9,[b] 4.3[d]

[a]Data obtained by ICP-AES. [b]D (%) = percentage metal dispersion obtained from hydrogen chemisorption. [c]From TEM. [d]From XRD.

The X-ray diffraction patterns of the as-synthesized Si-SBA-3 and Al-SBA-3 materials are shown in Figure 2. The studied samples exhibit reflection peaks in the low-angle region, characteristic of mesostructures. The presence of three Bragg angles can be distinguished in hexagonal lattice symmetry, typical of the SBA-3 structure. Moreover, XRD patterns indicate that the hexagonally ordered structure of SBA-3 was persistent after the modification procedure. A prominent peak at hkl = [100] as well as weaker peaks of [110] and [200] were observed in Al-SBA-3, which allowed us to corroborate that the

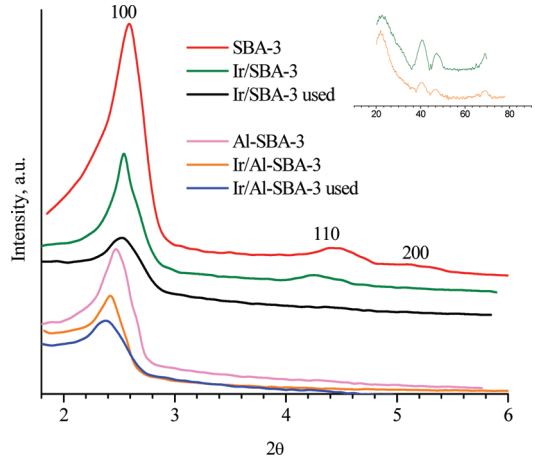

Figure 2. XRD patterns of synthesized SBA-3, Al-SBA-3, Ir/SBA-3, and Ir/Al-SBA-3 samples. Inset: High-angle XRD of Ir/SBA-3 and Ir/Al-SBA-3.

obtained mesoporous sample had a highly ordered pore system with a high porosity.[46]

The XRD powder patterns measured for the calcined (550 °C) MCM-41 solids are shown in Figure 3. In general, the

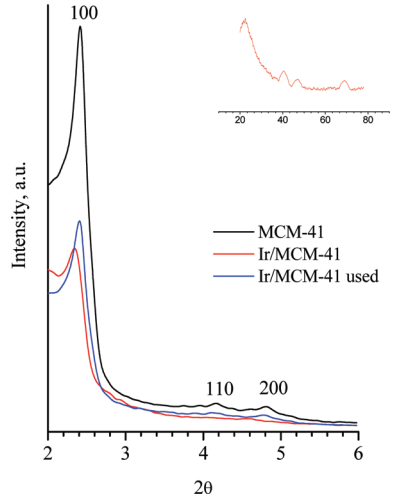

Figure 3. XRD patterns of synthesized MCM-41and Ir/MCM-41 samples. Inset: High-angle XRD of Ir/MCM-41.

samples show a distinct broad peak at 2.2° < 2θ < 3°, accounting for the Bragg plane (100), which is typical of the hexagonal structure of MCM-41 materials. Another characteristic peak of mesoporous MCM-41 materials can be observed at 3.9° < 2θ < 4.5° and 4.5° < 2θ < 5.2°; for these samples, it is a rather flat peak, corresponding to the (110) and (200) reflections, respectively.

The Miller indices indicate that the ordered mesoporous structure was preserved after the incorporation of iridium. The a_0 values for all of the samples are listed in Table 1.

In line with these results, a characteristic first peak is still observed in the XRD patterns of the three materials (Figures 1−3). The XRD results suggest that the mesoporous structures of the materials were maintained during the course of the preparation of Ir-modified catalysts. However, a significant decrease in intensity and broadening after Ir deposition suggests some loss in the periodicity of the pore structure.

dx.doi.org/10.1021/ie202727r | Ind. Eng. Chem. Res. 2012, 51, 7185−7195

Therefore, an obstruction of the support pores after metal deposition can be assumed to occur in these catalysts.

One can also observe in the figures a pattern for used Ir/mesoporous samples (after the catalytic test). This fact demonstrates that the structure remains unalterable, even after three cycles of reaction.

High-angle XRD analyses of Ir/SBA-16, Ir/SBA-3, Ir/Al-SBA-3, and Ir/MCM-41 catalysts are shown in the insets of Figures 1−3. For the application of the Scherrer formula, we employed the Bragg angles at 40°, 47°, and 69°, corresponding to the [111], [200], and [220] diffractions planes, respectively, of iridium. The average diameters of the iridium particles obtained by the Scherrer formula are reported in Table 1. The validity of this hypothesis is justified by the closely similar values for the average metal particle size obtained from H_2 chemisorption and TEM.

TEM. The TEM investigation provides direct evidence for the locations of and dimensional information about the Ir nanoparticles. The TEM images for Ir/SBA-3, Ir/Al-SBA-3, and Ir/MCM-41 are presented in parts a−c, respectively, of Figure 4. The TEM and XRD results suggest that, the mesoporous

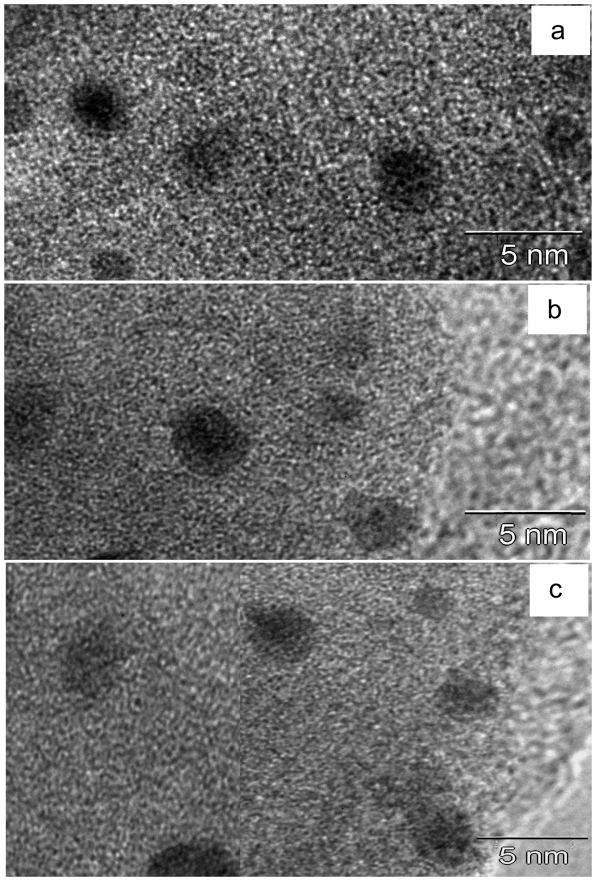

Figure 4. TEM images of (a) Ir/SBA-3, (b) Ir/Al-SBA-3, and (c) Ir/MCM-41.

structure of SBA-3, Al-SBA-3 and MCMC-41 was maintained during the course of preparing the catalyst. After introduction of Ir nanoparticles, the hexagonal structure of the catalyst was still observed, and fine Ir particles appeared in all materials. Interestingly, most of the Ir particles with sizes of only a few nanometers were uniformly dispersed in the mesoporous materials.

The results of ICP-AES elemental analysis, which was employed to determine the composition of the Al-SBA-3 sample, indicated that the amounts of metal (Al) in the final Al-SBA-3 product were in close agreement with the theoretical value, Si/Al = 19.8. The BET specific surface area decreased with the Al content, from 1024 m^2/g for SBA-3 to 770 m^2/g for Al-SBA-3, because of the occupation of guest species on the surface of the pores, as well as the nonuniform contribution of the additional mass Al_2O_3 in the sample.

The Al insertion in Al-SBA-3 was determined in a previous work by ^{27}Al nuclear magnetic resonance (NMR) spectroscopy, and the acidity was monitored by infrared spectroscopy of pyridine adsorption/desorption.[46] The ^{27}Al NMR results indicated that Al was effectively incorporated into the framework of the SBA-3 material by the postsynthesis method. The bridging hydroxyl ($Si_3O-Al-OH$) acid sites were observed after the adsorption of basic probe molecules, such as pyridine; this fact strongly supports the presence of Brønsted acid sites (Table 2).

Table 2. Quantification of Brønsted and Lewis Sites in Al-SBA-3 (Si/Al = 20) and Ir/Al-SBA-3 at Different Temperatures

	Brønsted (μmol of Py/g)		Lewis (μmol of Py/g)		Brønsted/Lewis	
temperature	Al-SBA-3	Ir/Al-SBA-3	Al-SBA-3	Ir/Al-SBA-3	Al-SBA-3	Ir/Al-SBA-3
373	127	98	53	46	2.40	2.13
473	126	65	48	42		
573	119	53	43	38	2.75	1.39
673	84	46	41	36		

A quantitative evaluation of acid sites, both Brønsted and Lewis, for samples under different desorption temperatures is reported in Table 2. The hydrogen-bonded pyridine bands decreased faster when the samples were outgassed at low temperatures. However, the strength of the acid sites was high because the bands decreased slowly when desorption occurred (373, 473, 573, and 673 K) and pyridine adsorbed onto Lewis and Brønsted acid sites still existed when samples desorbed at 673 K. One can assume that the incorporation of Al into the SBA-3 matrix gives rise to a greater amount of moderately strong Brønsted acid sites in the form of Si−O(H)−Al bridges. Pyridinium ions (PyH^+) on Brønsted sites also decreased with heat treatment.[46] However, this reduction appeared to be relatively lower than Lewis acid sites at 373 K, increasing the ratio of Brønsted acid sites compared to Lewis acid sites at higher desorption temperatures. In the case of Ir/Al-SBA-3 catalyst, we observed a lower amount of total acidic sites. Furthermore, the ratio of Brønsted/Lewis sites decreased. The decrease of Lewis acid sites appeared to be relatively lower than the decrease of Brønsted acid sites at all studied temperatures, thus increasing the Brønsted/Lewis acid site ratio. This fact indicates the interaction of Ir with Brønsted sites and the absent of new Brønsted sites created by the incorporation of Ir. The results of pyridine chemisorptions presented here are useful to distinguish the precise nature of the acidic sites that remained after Ir had been incorporated using an organic iridium source. This supports the idea of the bifunctional character of this catalyst, iridium active sites and Brønsted acid sites of the support, making it active for hydrogenation of tetralin and

dx.doi.org/10.1021/ie202727r | Ind. Eng. Chem. Res. 2012, 51, 7185−7195

avoiding the cracking activity, because of the moderate quantities and strength of acidity.

The content of iridium in the catalysts was determined by ICP-AES, and the iridium dispersion in the reduced catalysts was also determined by pulse H_2 adsorption at 22 °C (Table 1).

The average diameters of the iridium particles obtained by Scherrer's formula are closely similar values to the average metal particle size obtained from H_2 chemisorption and TEM. The incorporation of metal into the structure therefore leads to a slight decrease in the surface area but maintains the pore diameter and the mesoporous character. However, the values agreed sufficiently well to allow us to conclude that all of the metal was accessible to hydrogen and that no side phases formed. In summary, in these various iridium-metal-containing systems, the metal particle size depends on the metal content, the support, the surfactant and the method of incorporation.

After catalytic reaction with tetralin, the metal particle size estimated from the width of the X-ray diffraction line was unchanged. The Ir/SBA-3 catalyst with the 1 wt % iridium content presented a high capacity for hydrogen chemisorption, consistent with a high Ir dispersion.

Catalytic Activity. Despite industrial conditions that use high pressure and temperature, in this work, we address more active catalysts to perform under mild conditions and in a batch reactor. The catalytic activities of the synthesized samples were compared with that of a commercial $NiMo/Al_2O_3$ presulfided catalyst and Ir/Al_2O_3, using Topsoe M-80T γ-alumina with the same percentage of iridium, prepared according to the same procedure as used for the other samples, as detailed in the Experimental Section.

The hydrogenation reactions of tetralin were carried out at 250 °C and 15 atm in the presence of traces of DBT. The major products were *trans*-decalin, *cis*-decalin, and naphthalene. *trans*-Decalin was the product with the highest initial selectivity, followed by *cis*-decalin and then naphthalene. The trans isomer is expected to be favored based on thermodynamic calculations. Dehydrogenation of tetralin to naphthalene also took place during the hydrogenation of tetralin, even though the experiments were performed far below the conditions of thermodynamic equilibrium. Naphthalene formation was found to be dependent on the tetralin concentration and the hydrogenation rate. A high tetralin concentration together with a low hydrogenation rate favored naphthalene formation. Dehydrogenation was nevertheless a minor reaction, and only traces of naphthalene were formed. Sapre and Gates[1] and Korre et al.[6] reported a similar reversible dehydrogenation−hydrogenation reaction for tetralin and naphthalene on a sulfided CoMo catalyst. The decalins appeared to be unreactive under these conditions.

To study the behavior of the samples in the absence and presence of S, the computation of kinetic parameters can be useful; the data can be used to provide a better value for the constraints used to obtain the rate constants in the model. The generalized Langmuir−Hinshelwood rate equation can be used to represent the behavior of different catalysts in the hydrogenation of tetralin.

Kinetic Calculations. First-order tetralin hydrogenation rate constants based on the rate of tetralin disappearance were calculated using the integral method. The tetralin conversion exhibited first-order behavior in a plot of $\ln(C_{TL}/C_{TL,0})$ versus time, where C_{TL} is the tetralin concentration and $C_{TL,0}$ is the initial tetralin concentration (Figure 5). The slope and correlation coefficient were calculated by least-squares fitting.

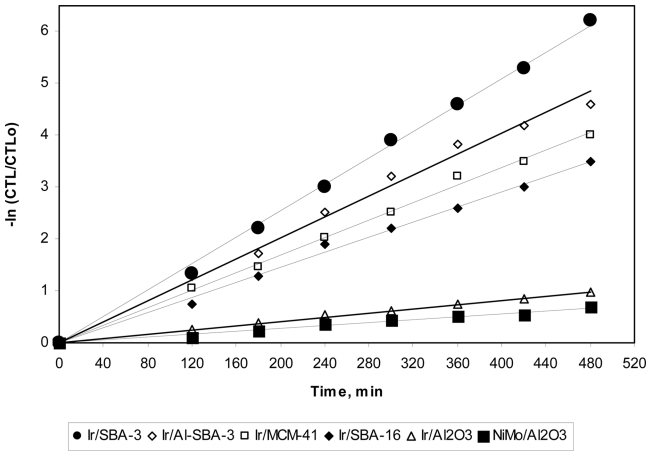

Figure 5. First-order behavior of tetralin hydrogenation without DBT at 250 °C and 15 atm.

In all cases, we obtained correlation coefficients higher than 0.96. *trans*-Decalin and *cis*-decalin were observed as the main products of the tetralin hydrogenation reaction (more than 98%). The semiempirical kinetic model proposed is the generalized Langmuir−Hinshelwood model for hydrogenation. For tetralin hydrogenation, the reaction rate is given by

$$r_{TL} = \frac{kK_{TL}C_{TL}}{1 + K_{TL}C_{TL}} \frac{K_{H_2}C_{H_2}}{1 + K_{H_2}C_{H_2}} \quad (2)$$

where r_{TL} is the rate of tetralin conversion to decalins, C_{TL} is the tetralin concentration, C_{H_2} is the hydrogen concentration, k is the rate constant, and K_{TL} and K_{H_2} are the adsorption equilibrium constants of the individual compounds. Under our experimental conditions, $K_{H_2}C_{H_2} \gg 1$, so this kinetic equation can be simplified to

$$r_{TL} = \frac{kK_{TL}C_{TL}}{1 + K_{TL}C_{TL}} \quad (3)$$

The kinetic calculations exhibited first-order behavior with respect to the tetralin concentration, and the value of the $K_{TL}C_{TL}$ product was close to 0. Expressing kK_{TL} as k_{TL}, eq 3 can be further simplified to

$$r_{TL} = k_{TL}C_{TL} \quad (4)$$

The values obtained for k_{TL} at 250 °C (Figure 5) using the integral method, already described, are reported in Table 3. These values were used as a reference for the results obtained in experiments in which this reaction was inhibited by sulfur.

Table 3. Kinetic Constants for the Different Samples Derived from the Kinetic Analysis

sample	kinetic constant k_{TL} [L/(min mmol)]	DBT adsorption constant K (L/mmol)
Ir/SBA-3	0.0128	93
Ir/Al-SBA-3	0.0101	114
Ir/MCM-41	0.0085	122
Ir/SBA-16	0.0073	130
Ir/Al_2O_3	0.003	112
$NiMo/Al_2O_3$ (Criterion DN-200)	0.0014	72

dx.doi.org/10.1021/ie202727r | Ind. Eng. Chem. Res. 2012, 51, 7185−7195

Control of the Kinetic Regime. A set of experiments was performed to check the absence of intraparticle and interphase mass-transfer limitations. Catalyst particles of different sizes (0.2, 0.4, 0.6, and 0.8 mm) were tested, and the results indicated that a kinetic regime was established in all cases.

Kinetic Model for Tetralin Inhibition by Sulfur. The hydrogenation of tetralin was carried out at 250 °C and 15 atm in the presence of dibenzothiophene (concentration equivalent to 100 ppm as sulfur). The inhibiting effect in tetralin hydrogenation was studied according to the method of La Vopa and Satterfield,[2] and the following equation was proposed

$$r_{TL} = \frac{k_{TL}C_{TL}}{1 + K_i C_i} \quad (5)$$

where r_{TL} is the pseudo-first-order rate constant for the reaction inhibited by sulfur compounds, K_i is the apparent sulfur compound adsorption equilibrium constant (L/mmol) and represents the behavior of the sulfur compound that contributes to the inhibition, and C_i is the initial DBT concentration (mmol/L). The results of these experiments (Figure 6) were fitted to a pseudo-first-order rate equation,

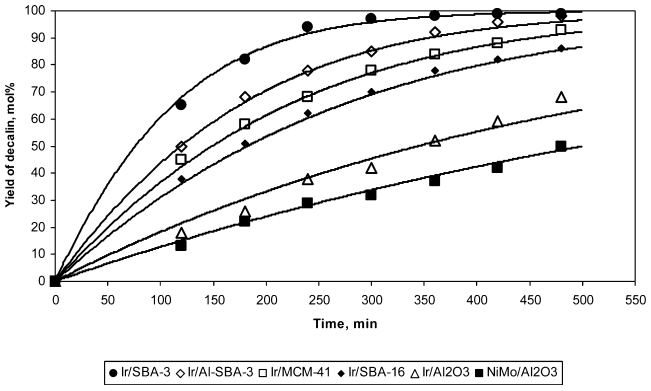

Figure 6. Kinetics of the hydrogenation of tetralin at T = 250 °C, P = 15 atm, 360 rpm, with 100 ppm of sulfur as DBT added to the feed. The lines were obtained by fitting the kinetic curves derived from the model to the experimental data ($F = 1.08^{-3}$).

with correlation coefficients (R^2) better than 0.96 in all cases. The excellent representation of the experimental results by a pseudo-first-order rate equation implies that the inhibition effect was approximately constant during each test. The inhibiting strength did not seem to be affected by the conversion of the parent sulfur compound; this behavior suggests that the coverage of the available active sites by sulfur compounds was established in the early stages of the reaction and remained nearly constant throughout the experiment, probably because of the slow desorption kinetics of these compounds.[72,73] Therefore, the variation in the sulfur compound concentration along time was not considered in the development of the model. The parameter estimation of the kinetic model was performed with the Powell version of the Levenberg–Marquardt algorithm. The differential equation was solved using the EPISODE package of Scientist. The objective function (eq 6) was the sum of the squares of the differences between the experimental and calculated yields of decalin versus the time of reaction, for each particular inhibitor (Figure 6)

$$F = \sum_{1}^{n} (y_{exp} - y_{cal})^2 \quad (6)$$

The catalytic results revealed the good performance of these monometallic catalysts at low temperatures, where high conversions and high yields of hydrogenation products were obtained, improving on the behavior displayed by the commercial catalyst. It is noteworthy that these catalysts require lower contact times and hydrogen/tetralin molar ratios than the NiMo catalyst, thus reducing the cost of the process if used in future industrial applications.

According with the catalytic tests, the synthesized Ir/SBA-3 sample was the most active catalyst in this reaction, taking into account the kinetic constant values (Table 3). Differences in activity could be due to the better iridium dispersion obtained on SBA-3 used as the support.

It seems therefore that the order of the activity was influenced by the type of the support, which can affect the strength of the interaction with the noble-metal precursor. The decreasing trend with increasing Ir cluster size is well apparent. Hydrogen chemisorption, TEM, and XRD measurements of these catalysts in the reduced state suggest that the higher activities of the samples with smaller Ir sizes can be explained by higher Ir dispersions.[50]

According to our previous work,[61] the selective conversion of tetralin to decalin using 5 wt % Ir/SBA-16 was higher than that obtained with 5 wt % Ir/Al_2O_3 and 60% higher than that obtained with Criterion 424 NiMo/Al_2O_3. The turnover numbers suggested that the higher conversion levels were due to the higher dispersion of Ir atoms as the active centers of the reaction. The 5 wt % iridium-containing SBA-16 also showed a higher activity even in the presence of sulfur than a typical NiMo catalyst.

From the literature, the loading of 5% Ir on a mesoporous FSM-16 silicate led to a thiophene HDS activity almost equivalent to those of the CoMo and NiMo/FSM-16 systems and lower than that of a commercial CoMo/Al_2O_3 catalyst.[74] Also, 5% Ir deposited on an Al-pillared montmorillonite[75] and 11% Ir on Al_2O_3[76] were less active in the HDS of thiophene than the CoMo/Al_2O_3 catalyst. It is likely that the lower activities of these Ir catalysts could be associated with lower Ir dispersion. The carbon-supported Ir catalyst (16% Ir) and commercial CoMo/Al_2O_3 and NiMo/Al_2O_3 catalysts have been compared in two HDS reactions. The Ir/C catalyst showed much higher HDS activity than CoMo and NiMo/Al_2O_3 catalysts in the simultaneous HDS of thiophene and HDN of pyridine.[29] The activity of the Ir/Al_2O_3 catalyst (4.8% Ir) per mole of Ir was approximately 3 times higher than that of the CoMo catalyst and about 2 times higher than that of the NiMo catalyst. Substantially greater differences in the specific activities of Ir/Y-zeolite (0.8% Ir) and NiMo/Al_2O_3 catalysts in the HDN of quinoline were observed by Harvey and Pratt.[30]

In this case, all of the synthesized samples were far more active than NiMo catalyst (up to 10 times faster in the case of Ir/SBA-3). The good activity of Ir/Al-SBA-3 compared with the other synthesized samples as Ir-containing MCM or SBA-16 could be due to the good dispersion of Ir and the acidic character of this catalyst.[46] The bifunctional character of this catalyst, namely, the participation of both the active sites of Ir and the Brønsted acid sites of the support, make it active for hydrogenation of tetralin. This hypothesis is in agreement with the findings of Klimova et al.,[37] who prepared NiMo catalysts supported on Al-containing SBA-16 molecular sieves by

dx.doi.org/10.1021/ie202727r | Ind. Eng. Chem. Res. 2012, 51, 7185–7195

grafting with $AlCl_3$ or $Al(i\text{-}PrO)_3$; the catalysts showed high activity in the HDS of refractory dibenzothiophenes [e.g., 4,6-dimethyldibenzothiophene (4,6-DMDBT)]. This was attributed to good dispersion of the Ni and Mo active phases and to the bifunctional character of the catalysts: active sites of the NiMoS phase and Brønsted acid sites of the support in the catalytic transformations of 4,6-DMDBT. Therefore, the high catalytic performance of these catalysts in the HDS of refractory DBTs was attributed to the synergism between the two types of active sites. The interaction of the Ni and Mo species with the support became stronger with Al loading in SBA-16 by postsynthetic aluminum grafting. In this case, the dispersion of sulfided Mo species increased. However, when SBA-16 was aluminated using $NaAlO_2$, NiMo catalysts with low surface area and activity were obtained. This indicates the importance of the method of aluminum incorporation into SBA-type materials and Al sources suitable for the preparation of supports for HDS catalysts.

In our case, it is possible to see that postsynthetic alumination of SBA-3 by reaction with $NaAlO_2$ led to a significant decrease in the surface area and total pore volume compared with the parent material. We also obtained a catalyst with a lower dispersion of iridium than the parent SBA-3 without aluminum. This trend in the activity with change in the Al-containing SBA-3 support would be the result of a metal−support interaction that was too strong, as in the case of the Ir/Al-SBA-3 catalyst, that made the reduction of Ir species more difficult.

Figure 6 shows the activities of the different samples included in this study in the presence of DBT. The activity was found to increase in the order $NiMo/Al_2O_3$ < Ir/Al_2O_3 < Ir/SBA-16 < Ir/MCM-41 < Ir/Al-SBA-3 < Ir/SBA-3. The inhibiting effect of sulfur is strong at concentrations as low as 100 ppm, but Ir-SBA-3 was still more active than the commercial NiMo/alumina catalyst (i.e., the mole percentage conversion of tetralin obtained at the same conditions was 65% higher at 4 h of reaction).

Thus, the inhibition behavior seems to be related to the strong adsorption of the specific sulfur compound directly on the catalyst surface.[77−79] To elucidate this relationship, the adsorption constants were determined. Calculated Langmuir adsorption constants for all of the samples tested are listed in the second column of Table 3, for the data obtained at 250 °C. Among these compounds, the adsorption strength increased in the order $NiMo/Al_2O_3$ < Ir/SBA-3 < Ir/Al_2O_3 < Ir/Al-SBA-3 < Ir/MCM-41 < Ir/SBA-16.

The lower sulfur tolerance of Ir in SBA-16 or MCM-41 as compared to SBA-3 can be explained by a stronger adsorption of sulfur on the Ir. The resistance to poisoning depends, to a large extent, on the nature of the support, as well as the size, structure, and location of the metal particles, and many points are still under discussion. The metal−support interaction beings about an increase in the amount of electron-deficient metal sites, which improves the sulfur tolerance by reducing irreversible electrophilic sulfur adsorption and thereby reducing sulfur-induced coke formation. Electron-deficient species in bimetallic catalysts are claimed by a number of researchers to be responsible for the sulfur tolerance of such catalysts against the electron-acceptor character of the sulfur.[80−82]

The formation of iridium sulfide might be possible. It has been widely recognized in the literature that this "iridium sulfide" is fairly active in HDS reactions,[74−76] especially when the support is acidic and iridium is interacting strongly with the electron-deficient support. This weakens its interaction with sulfur and therefore allows superficial sulfur vacancies to be created, where new DBT molecules can undergo HDS reactions. This could be an explanation for the good activity of Ir/Al-SBA-3.

These results clearly indicate that the interaction of sulfur with the metallic particles is very weak, which points to a low level of back-bonding of electron density from the metallic particles to the sulfur atoms. This means that there is a strong metal−support interaction making these metal particles electron-deficient. This is probably due to the very small Ir particle size, as evidenced by H_2 chemisorption, XRD, and TEM, which, according to Foger and Anderson,[34] is significantly influenced by the support.

However, these catalysts present good activity and thiotolerance better than those of other catalysts described in the literature, which exhibited higher deactivation by sulfur,[83−91] although it is difficult to compare our results with those obtained using other catalysts because they were tested under different experimental conditions.

CONCLUSIONS

The Ir-SBA-3 catalyst synthesized in this work had the highest activity measured in tetralin hydrogenation under mild conditions. The good activity was correlated with higher Ir dispersion on the SBA-3 mesostructured material used as the support, with more active metal sites exposed to the reactant. A kinetic model was successfully applied to the hydrogenation of tetralin in the presence of sulfur. The hydrogenation rates were useful in determining the most active catalyst. The hydrogenation rates of tetralin were lower when sulfur was present in the mixture. The inhibition was described reasonably well by Langmuir−Hinshelwood kinetics. The adsorption strengths of the inhibitors increased in the order $NiMo/Al_2O_3$ < Ir/SBA-3 < Ir/Al_2O_3 < Ir/Al-SBA-3 < Ir/MCM-41 < Ir/SBA-16. Even though the DBT adsorption constant for NiMo is lower than that for Ir/SBA-3, the latter catalyst is far more active for this hydrogenation reaction. The sulfur tolerance of the Ir/SBA-3 catalyst is sufficiently high to envisage use of this catalyst in the final stages of a refinery process producing diesel fuel of high cetane number by hydrodearomatization.

AUTHOR INFORMATION

Corresponding Author

*E-mail: abeltramone@scdt.frc.utn.edu.ar.

Notes

The authors declare no competing financial interest.

ACKNOWLEDGMENTS

We thank CONICET Argentina, PIP no. 112-200801-00388 (2009-2012), and MINCyT Cba. 1210/07 (2007-2012).

REFERENCES

(1) Sapre, A. V.; Gates, B. C. Hydrogenation of aromatic hydrocarbons catalyzed by sulfided $CoO−MoO_3/\gamma\text{-}Al_2O_3$. Reactivities and reaction networks. *Ind. Eng. Chem. Process Des. Dev.* **1981**, *20*, 68−73.

(2) La Vopa, V.; Satterfield, C. N. Poisoning of thiophene hydrodesulfurization by nitrogen compounds. *J. Catal.* **1988**, *110*, 375−387.

(3) Sarbak, Z. Catalytic hydrodenitrogenation of carbazole and some of its partially hydrogenated intermediate products. *React. Kinet. Catal. Lett.* **1986**, *32*, 449−455.

(4) Beltramone, A.; Resasco, D.; Alvarez, W.; Choudhary, T. Simultaneous Hydrogenation of Multiring Aromatic Compounds over NiMo Catalyst. *Ind. Eng. Chem. Res.* **2008**, *47*, 7161−7166.
(5) Beltramone, A.; Crossley, S.; Resasco, D.; Alvarez, W.; Choudhary, T. Inhibition of the Hydrogenation and Hydrodesulfurization Reactions by Nitrogen Compounds over $NiMo/Al_2O_3$. *Catal. Lett.* **2008**, *123*, 181−185.
(6) Korre, S. C; Klein, M. T.; Quann, R. J. Polynuclear Aromatic Hydrocarbons Hydrogenation: Part 1. Experimental Reaction Pathways and Kinetics. *Ind. Eng. Chem. Res.* **1995**, *34*, 101−107.
(7) Jacquin, M.; Jones, D.; Rozière, J.; Jiménez López, A.; Rodríguez-Castellón, E.; Trejo Menayo, J.; Lenarda, M.; Storaro, L.; Vaccari, A.; Albertazzi, S. Cetane improvement of diesel with a novel bimetallic catalyst. *J. Catal.* **2004**, *228*, 447−459.
(8) Kukes, S. G.; Clark, F. T.; Hopkins, D.; Green, L. M. (Amoco Corporation). Distillate hydrogenation. U.S. Patent 5,151,172. 1992.
(9) Kukes, S. G.; Clark, F. T.; Hopkins, D. (Amoco Corporation). Distillate hydrogenation. U.S. Patent 5,147,526, 1992.
(10) Clark, F. T.; Kukes, S. G.; Hopkins, D. (Amoco Corporation). Distillate hydrogenation. U.S. Patent 5,271,828, 1993.
(11) Kukes, S. G.; Clark, F. T.; Hopkins, D. (Amoco Corporation). Distillate hydrogenation catalyst. U.S. Patent 5,308,814, 1994.
(12) Winquist, B. H. C.; Milam, S. N.; Murray, B. D.; Ryan, R. B. (Shell International Research Maatschappij B.V.). Hydrogenation catalyst and process. European Patent 0,519,573 A1, 1992.
(13) Breckenridge, L. L.; Del Rossi, K. J.; Huss, A.; Kennedy, C. R.; Kirker, G. X. (Mobil Oil Corporation). Combined paraffin isomerization/ring opening process. U.S. Patent 5,382,730, 1995.
(14) Del Rossi, K. J.; Jablonski, G. A.; Marler, D. O. (Mobil Oil Corporation). Process for cetane improvement of distillate fractions. International Patent WO 95/28459, 1995.
(15) Van Thillo, H.; Bodart, P.; Lamotte, C.; Grootjans, J. (Fina Research S.A.). Silica-alumina carriers preparation, hydrogenation catalysts preparation therewith and their use for aromatics hydrogenation. European Patent 0,669,162 A1, 1995.
(16) Vaarkamp, M.; Reesink, B. H.; Berben, P. H. (Engelhard Corporation). Process for hydrogenation, hydroisomerization and/or hidrodesulfurization of a sulfur contaminant containing feedstock. International Patent WO 98/35754, 1998
(17) Lucien, J. P.; Van Den Berg, G. G.; Van Hooijdonk, H. M. J. H.; Gjers, M.; Thielsman, G. L. B. *Catalyst Hydroprocessing of Petroleum and Distillates*; Marcel Dekker: New York, 1994; p 291.
(18) McVicker, G. B.; Touvelle, M. S.; Hudson, C. W.; Vaughan, D. E. W.; Daage, M.; Hantzer, S.; Klein, D. P.; Ellis, E. S.; Cook, B. R.; Feeley, O. C.; Baumgartner, J. E. (Exxon Research and Engineering Company). Process for selectively opening naphthenic rings. U.S. Patent 5,763,731, 1998
(19) Hantzer, S.; Touvelle, M. S.; Chen, J. (Exxon Research and Engineering Company). Selective opening of five and six membered rings. International Patent WO 97/09289, 1997.
(20) Touvelle, M. S.; McVicker, G. B.; Daage, M.; Hantzer, S.; Hudson, C. W.; Klein, D. P.; Vaughan, D. E. W.; Ellis, E. S.; Chen, J. (Exxon Research and Engineering Company). Process for selectively opening naphtenic rings. International Patent WO/09290, 1997.
(21) Cunha, D.; Cruz, G. Hydrogenation of benzene and toluene over Ir particles supported on γ-Al_2O_3. *Appl. Catal. A: Gen.* **2002**, *236*, 55−66.
(22) McVicker, G.; Daage, M.; Touvelle, M.; Hudson, C.; Klein, D.; Baird, W.; Cook, B.; Chen, J.; Hantzer, S.; Vaughan, D.; Ellis, E.; Feeley, O. Selective Ring Opening of Naphthenic Molecules. *J. Catal.* **2002**, *210*, 137−148.
(23) Arribas, M.; Concepción, P.; Martínez, A. The role of metal sites during the coupled hydrogenation and ring opening of tetralin on bifunctional Pt(Ir)/USY catalysts. *Appl. Catal. A: Gen.* **2004**, *267*, 111.
(24) Nylen, U.; Delgado, J. F.; Järås, S.; Boutonnet, M. Low and high-pressure ring opening of indan over 2 wt.% Pt, Ir and bi-metallic $Pt_{25}Ir_{75}$/boehmite catalysts prepared from microemulsion systems. *Appl. Catal. A: Gen.* **2004**, *262*, 189−200.
(25) Frety, R.; da Silva, P.; Guenin, M. Supported iridium catalysts: Comparison between resistance to sulphur poisoning and hydrodesulphurization properties. *Appl. Catal. A: Gen.* **1990**, *57*, 99.
(26) Dees, M. J.; den Hartog, A. J.; Ponec, V. Identification of active sites of reforming catalysts by poisoning. *Appl. Catal. A: Gen.* **1991**, *72*, 343.
(27) Pecoraro, T. A.; Chianelli, R. R. Hydrodesulfurization catalysis by transition metal sulfides. *J. Catal.* **1981**, *67*, 430.
(28) Eijsbouts, S.; de Beer, V. H. J.; Prins, R. Periodic trends in the hydrodenitrogenation activity of carbon-supported transition metal sulfide catalysts. *J. Catal.* **1988**, *109*, 217.
(29) Vit, Z.; Zdrazïil, M. Simultaneous hydrodenitrogenation of pyridine and hydrodesulfurization of thiophene over carbon-supported platinum metal sulfides. *J. Catal.* **1989**, *119*, 1−7.
(30) Harvey, T. G.; Pratt, K. C. Hydrodenitrogenation Using Ternary Metal Catalysts on Mixed Zeolite-γ-Alumina Supports. *Appl. Catal. A: Gen.* **1989**, *47*, 335−341.
(31) Cinibulk, J.; Vít, Z. Hydrodenitrogenation of pyridine over alumina-supported iridium catalysts. *Appl. Catal. A: Gen.* **1999**, *180*, 15−23.
(32) Rocha, A. S.; Moreno, E. L.; da Silva, G. P. M.; Zotin, J. L.; Faro, A. C., Jr. Tetralin hydrogenation on dealuminated Y zeolite-supported bimetallic Pd−Ir catalysts. *Catal. Today* **2008**, *133*−*135*, 394−399.
(33) Dees, M. J.; den Hartog, A. J.; Ponec, V. Identification of active sites of reforming catalysts by poisoning. *Appl. Catal.* **1991**, *72*, 343−360.
(34) Foger, K.; Anderson, J. R. Hydrocarbon reactions on supported iridium catalysts. *J. Catal.* **1979**, *59*, 325−339.
(35) Dhar, G. M.; Kumaran, G. M.; Kumar, M.; Rawat, K. S.; Sharma, L. D.; Raju, B. D.; Rama Rao, K. S. Physico-chemical characterization and catalysis on SBA-15 supported molybdenum hydrotreating catalysts. *Catal. Today* **2005**, *99*, 309−314.
(36) Vradman, L.; Landau, M. V.; Herskowitz, M.; Ezersky, V.; Talianker, M.; Nikitenko, S.; Koltypin, Y.; Gedanken, A. High loading of short WS_2 slabs inside SBA-15: Promotion with nickel and performance in hydrodesulfurization and hydrogenation. *J. Catal.* **2003**, *213*, 163.
(37) Klimova, T.; Lizama, L.; Amezcua, J. C.; Roquero, P.; Terrés, E.; Navarrete, J.; Dominguez, J. M. New NiMo catalysts supported on Al-containing SBA-16 for 4,6-DMDBT hydrodesulfurization: Effect of the alumination method. *Catal. Today* **2004**, *98*, 141−150.
(38) Amezcua, J. C.; Lizama, L.; Salcedo, C.; Puente, I.; Dominguez, J. M.; Klimova, T. NiMo catalysts supported on titania-modified SBA-16 for 4,6-dimethyldibenzothiophene hydrodesulfurization. *Catal. Today* **2005**, *107/108*, 578−588.
(39) Nava, R.; Ortega, R. A.; Alonso, G.; Ornelas, C.; Pawelec, B.; Fierro, J. L. G. CoMo/Ti-SBA-15 catalysts for dibenzothiophene desulfurization. *Catal. Today* **2007**, *127*, 70−84.
(40) Zhao, D.; Feng, J.; Huo, Q.; Melosh, N.; Fredrickson, G. H.; Chmelka, B. F.; Stucky, G. D. Triblock Copolymer Syntheses of Mesoporous Silica with Periodic 50 to 300 Angstrom Pores. *Science* **1998**, *279*, 548−552.
(41) Mesa, M.; Sierra, L.; Guth, J. Contribution to the study of the formation mechanism of mesoporous SBA-15 and SBA-16 type silica particles in aqueous acid solutions. *Microporous Mesoporous Mater.* **2008**, *112*, 338−350.
(42) Anunziata, O.; Beltramone, A.; Martínez, M.; López-Belon, L. Synthesis and characterization of SBA-3, SBA-15, and SBA-1 nanostructured catalytic materials. *J. Colloid Sci.* **2007**, *315*, 184−90.
(43) Hu, W.; Luo, Q.; Su, Y.; Chen, L.; Yue, Y.; Ye, C.; Deng, F. Acid sites in mesoporous Al-SBA-15 material as revealed by solid-state NMR spectroscopy. *Microporous Mesoporous Mater.* **2006**, *92*, 22−30.
(44) Luan, Z.; Hartmann, M.; Zhao, D.; Zhou, W.; Kevan, L. Alumination and ion exchange of mesoporous SBA-15 molecular sieves. *Chem. Mater.* **1999**, *11* (6), 1621−1627.
(45) Klimova, T.; Reyes, J.; Gutierrez, O.; Lizama, L. Novel bifunctional NiMo/Al-SBA-15 catalysts for deep hydrodesulfurization: Effect of support Si/Al ratio. *Appl. Catal. A: Gen.* **2008**, *335*, 159−171.

(46) Anunziata, O. A.; Martínez, M. L.; Gómez Costa, M. Characterization and acidic properties of Al-SBA-3 mesoporous material. *Mater. Lett.* **2010**, *64*, 545−548.
(47) Zhao, D.; Huo, Q.; Feng, J.; Chmelka, B. F.; Stucky, G. D. Nonionic Triblock and Star Diblock Copolymer and Oligomeric Surfactant Syntheses of Highly Ordered, Hydrothermally Stable, Mesoporous Silica Structures. *J. Am. Chem. Soc.* **1998**, *120*, 6024−6036.
(48) Mesa, M.; Sierra, L.; Patarin, J.; Guth, J.-L. Morphology and porosity characteristics control of SBA-16 mesoporous silica. Effect of the triblock surfactant Pluronic F127 degradation during the synthesis. *Solid State Sci.* **2005**, *7*, 990−997.
(49) Furimsky, E. Selection of catalysts and reactors for hydroprocessing. *Appl. Catal. A: Gen.* **1998**, *171*, 177.
(50) Vít, Z. Iridium sulfide and Ir promoted Mo based catalysts. *Appl. Catal. A: Gen.* **2007**, *322*, 142−151.
(51) Frety, R.; Da Silva, P. N.; Guenin, M. Supported iridium catalysts: Comparison between resistance to sulphur poisoning and hydrodesulphurization properties. *Appl. Catal. A: Gen.* **1990**, *57*, 99−103.
(52) Navarro, R.; Pawelec, B.; Fierro, J. L. G.; Vasudevan, P. T.; Cambra, J. F.; Arias, P. L. Deep hydrodesulfurization of DBT and diesel fuel on supported Pt and Ir catalysts. *Appl. Catal. A: Gen.* **1996**, *137*, 269.
(53) Barbier, J.; Marecot, P.; Tifouti, L.; Guenin, M.; Frety, R. Thioresistance of supported metal catalysts: Structure sensitivity of hydrogen sulphide adsorption on $Pt/A1_20_3$, $Ir/A1_20_3$ and $Pt\text{-}Ir/A1_20_3$ catalysts. *Appl. Catal. A: Gen.* **1985**, *19*, 375−385.
(54) Matsui, T.; Harada, M.; Ichihashi, Y.; Bando, K.; Matsubayashi, N.; Toba, M.; Yoshimura, Y. Effect of noble metal particle size on the sulfur tolerance of monometallic Pd and Pt catalysts supported on high-silica USY zeolite. *Appl. Catal. A: Gen.* **2005**, *286*, 249−257.
(55) Cowan, R.; Høglin, M.; Reinink, H.; Jsebaert, J.; Chadwick, D. Influence of ammonia on thiophene HDS at high pressures over noble metal catalysts for deep HDS applications. *Catal. Today* **1998**, *45*, 381.
(56) Dhainaut, E.; Charcosset, H.; Cachet, Ch.; de Mourgues, L. Dibenzothiophene hydrodesulfurization by noble metal supported catalysts. *Appl. Catal. A: Gen.* **1982**, *2*, 75−86.
(57) Dees, M. J.; den Hartog, A. J.; Ponec, V. Identification of active sites of reforming catalysts by poisoning. *Appl. Catal. A: Gen.* **1991**, *72*, 343−360.
(58) Ponec, V. Catalysis by Alloys in Hydrocarbon Reactions. *Adv. Catal.* **1983**, *32*, 149−214.
(59) Barbier, J.; Marecot, P. Effect of presulfurization on the formation of coke on supported metal catalysts. *J. Catal.* **1986**, *102*, 21−28.
(60) Liua, Z.; Li, J.; Junaid, A. S. M. Knowledge and know-how in improving the sulfur tolerance of $deNO_x$ catalysts. *Catal. Today* **2010**, *153*, 95−102.
(61) Balangero Bottazzi, G. S.; Martinez, M. L.; Gomez Costa, M.; Anunziata, O.; Beltramone, A. Inhibition of the hydrogenation of tetralin by nitrogen and sulfur compounds over Ir/SBA-16. *Appl. Catal. A: Gen.* **2011**, *404* (1−2), 30−38.
(62) Kim, T.-W.; Ryoo, R.; Kruk, M.; Gierszal, K.; Jaroniec, M.; Kamiya, S.; Terasaki, O. Tailoring the Pore Structure of SBA-16 Silica Molecular Sieve through the Use of Copolymer Blends and Control of Synthesis Temperature and Time. *J. Phys. Chem. B* **2004**, *108*, 11480−11489.
(63) Luan, Z.; Hartmann, M.; Zhao, D.; Zhou, W.; Kevan, L. Alumination and Ion Exchange of Mesoporous SBA-15 Molecular Sieves. *Chem. Mater.* **1999**, *11*, 1621−1627.
(64) Kumar, D.; Schumacher, K.; du Fresne von Hohenesche, C.; Grün, M.; Unger, K. K. MCM-41, MCM-48 and related mesoporous adsorbents: Their synthesis and characterization. *Colloids Surf. A* **2001**, *187- 188*, 109−116.
(65) Taylor, A. *X-ray Metallography*; Chapman and Hall: London, 1942; p 530; Imelik, B.; Vedrine, J.C. In *Catalyst Characterisation, Physical Techniques for Solid Materials*; Imelik, B., Vedrine, J. C., Eds.; Plenum Press: New York, 1994; pp 690−691.
(66) van Huis, M.; van Veen, A.; Schut, H.; Eijt, S.; Kooi, B.; De Hosson, J. Structural properties of Au and Ag nanoclusters embedded in MgO. *Nucl. Instrum. Methods Phys. Res. B* **2002**, *191*, 442.
(67) Zhao, D.; Huo, Q.; Feng, J.; Chmelka, B. F.; Stucky, G. D. Nonionic Triblock and Star Diblock Copolymer and Oligomeric Surfactant Syntheses of Highly Ordered, Hydrothermally Stable, Mesoporous Silica Structures. *J. Am. Chem. Soc.* **1998**, *120*, 6024.
(68) Wu, S.; Han, Y.; Zou, Y. C.; Song, J. W.; Zhao, L.; Di, Y.; Liu, S. Z.; Xiao, F. S. Synthesis of Heteroatom Substituted SBA-15 by the "pH-Adjusting" Method. *Chem. Mater.* **2004**, *16*, 486.
(69) Aburto, J.; Ayala, M.; Bustos-Jaimes, I.; Montiel, C.; Terres, E.; Dominguez, J. M.; Torres, E. Stability and catalytic properties of chloroperoxidase immobilized on SBA-16 mesoporous materials. *Microporous Mesoporous Mater.* **2005**, *83*, 193.
(70) Cheng, C.-F.; Lin, Y.-C.; Cheng, H.-H.; Chen, Y.-C. The effect and model of silica concentrations on physical properties and particle sizes of three-dimensional SBA-16 nanoporous materials. *Chem. Phys. Lett.* **2003**, *382*, 496.
(71) Van Der Voort, P.; Benjelloun, M.; Vansant, E. F. Rationalization of the Synthesis of SBA-16: Controlling the Micro- and Mesoporosity. *J. Phys. Chem. B* **2002**, *106*, 9027.
(72) Furimsky, E.; Massoth, F. E. Deactivation of hydroprocessing catalysts. *Catal. Today* **1999**, *52*, 381.
(73) Laredo, G.; De los Reyes, J.; Cano, L.; Castillo, J. Inhibition effects of nitrogen compounds on the hydrodesulfurization of dibenzothiophene. *Appl. Catal. A: Gen.* **2001**, *207*, 103.
(74) Sugioka, M.; Andalaluna, L.; Morishita, S.; Kurosaka, T. Noble metals supported on mesoporous silicate FSM-16 as new hydrodesulfurization catalyst. *Catal. Today* **1997**, *39*, 61.
(75) Sugioka M.; Watanabe H. In *Proceedings of the 1998 International Symposium on Advanced Energy Technology, 2−4 February 1998, Sapporo, Japan*; 1998; p 247.
(76) Mangnus, P. J.; Riezebos, A.; van Langeveld, A. D.; Moulijn, J. A. Temperature-Programmed Reduction and HDS Activity of Sulfided Transition Metal Catalysts: Formation of Nonstoichiometric Sulfur. *J. Catal.* **1995**, *151*, 178.
(77) Dong, D.; Jeong, S.; Massoth, F. E. Effect of nitrogen compounds on deactivation of hydrotreating catalysts by coke. *Catal. Today* **1997**, *37*, 267.
(78) Muegge, B.; Massoth, F. E. In *Catalyst Deactivation*; Bartholomew, C. H., Butt, J. B., Eds.; Elsevier: Amsterdam, 1991; p 297.
(79) Yang, S. H.; Satterfield, C. N. Catalytic hydrodenitrogenation of quinoline in a trickle-bed reactor. Effect of hydrogen sulfide. *Ind. Eng. Chem. Process Des. Dev.* **1984**, *23*, 20.
(80) Dalla Betta, R. A.; Boudart, M. In *Proceedings of the 5th International Congress on Catalysis*; Hightower, J. W., Ed.; North Holland: Amsterdam, 1973; Vol. 2, 1329.
(81) Yoshimura, Y.; Toba, M.; Matsui, T.; Harada, M.; Ichihashi, Y.; Bando, K. K.; Yasuda, H.; Ishihara, H.; Morita, Y.; Kameoka, T. Active phases and sulfur tolerance of bimetallic Pd−Pt catalysts used for hydrotreatment. *Appl. Catal. A: Gen.* **2007**, *322*, 152−171.
(82) Lin, T. B.; Jan, C. A.; Chang, J. R. Aromatics reduction over supported platinum catalysts. 2. Improvement in sulfur resistance by addition of palladium to supported platinum catalysts. *Ind. Eng. Chem. Res.* **1995**, *34*, 4284.
(83) Pawelec, B.; Mariscal, R.; Navarro, R. M.; van Bokhorst, S.; Rojas, S.; Fierro, J. L. G. Hydrogenation of aromatics over supported Pt−Pd catalysts. *Appl. Catal. A: Gen.* **2002**, *225*, 223.
(84) Fujikawa, T.; Idei, K.; Ebihara, T.; Mizuguchi, H.; Usui, K. Aromatic hydrogenation of distillates over $SiO_2\text{-}Al_2O_3$-supported noble metal catalysts. *Appl. Catal. A: Gen.* **2000**, *192*, 253.
(85) Navarro, R.; Pawelec, B.; Trejo, J. M.; Mariscal, R.; Fierro, J. L. G. Hydrogenation of Aromatics on Sulfur-Resistant PtPd Bimetallic Catalysts. *J. Catal.* **2000**, *189*, 184.
(86) Yasuda, H.; Yoshimura, Y. Hydrogenation of tetralin over zeolite-supported Pd−Pt catalysts in the presence of dibenzothiophene. *Catal. Lett.* **1997**, *46*, 43.

(87) Petitto, C.; Giordano, G.; Fajula, F.; Moreau, C. Influence of the source of sulfur on the hydroconversion of 1-methylnaphthalene over a Pt−Pd/USY catalyst. *Catal. Commun.* **2002**, *3*, 15.
(88) Arribas, M. A.; Martínez, A. The influence of zeolite acidity for the coupled hydrogenation and ring opening of 1-methylnaphthalene on Pt/USY catalysts. *Appl. Catal. A: Gen.* **2002**, *230*, 203.
(89) Le Bihan, L.; Yoshimura, Y. Control of hydrodesulfurization and hydrodearomatization properties over bimetallic Pd−Pt catalysts supported on Yb-modifed USY zeolite. *Fuel* **2002**, *81*, 491.
(90) Rousset, J. L.; Stievano, L.; Cadete Santos Aires, F. J.; Geantet, C.; Renouprez, A. J.; Pellarin, M. Hydrogenation of Tetralin in the Presence of Sulfur over γ-Al_2O_3-Supported Pt, Pd, and Pd−Pt Model Catalysts. *J. Catal.* **2001**, *202*, 163.
(91) Costa Augusto, C. C.; Zotin, J. L.; Da Costa Faro, A. Effect of Sulfur or Nitrogen Poisoning on the Activity and Selectivity of Y-Zeolite-Supported Pt−Pd Catalysts in the Hydrogenation of Tetralin. *Catal. Lett.* **2001**, *75*, 37−43.